Applying Normally-off GaN HEMTs for Coreless High-frequency Wireless Chargers

Wei Qian, Xi Zhang, Yongsheng Fu, Juncheng Lu and Hua Bai

***Abstract*—Wide-bandgap (WBG) devices such as Gallium-Nitride (GaN) High Electron Mobility Transistors (HEMTs) have become popular in the power electronics industry as they offer a lower switching loss, higher thermal capability and higher power density than conventional silicon devices. As an attempt of applying WBG devices to the wireless charging technology, this paper adopts two different types of normally-off GaN HEMTs. One adopts the cascode structure provided by Transphorm Inc, operated under 800kHz to charge a battery pack on an electric scooter at 48 V/500W, with the air gap between the transceiver and receiver of ~10cm. The other is enhancement-mode GaN HEMTs provided by GaN Systems Inc, operated at ~6MHz to use one transceiver to charge multiple cell phones @~20W. Both of these chargers have no magnetic cores to reduce the cost and weight. Experimental results show both types of GaN HEMTs significantly increased the charging efficiency over conventional Si devices. Challenges of applying such fast-transition devices are discussed, e.g., common-source inductance and the gate-drive-loop parasitic.**

***Index Terms*—CoolMOS, GaN HEMT, Wide-bandgap semiconductor, wireless power transfer, zero voltage switching.**

I. INTRODUCTION

WPT has several advantages compared to wired solutions, as the usability, no wear of connections and the possibility to transfer power from one transmitter to multiple receivers and vice versa. The earliest occurrence of a Wireless Power Transfer (WPT) concept is attributed to Nikola Telsa, who in 1900 and 1914 published two patents for wirelessly transmitting electrical energy [1, 2]. Since then it was always an aim to get rid of the dependence on wired solutions for the power transmission. The next remarkable step was done nearly 100 years later at the MIT in 2006. A great progress was made by promoting WiTricity, transmitting 60 W with an efficiency of around 40 % over a distance of 2 meters, which gained attention all over the world [3]. The concept of WiTricity is that two objects having the same resonant frequency tend to exchange energy efficiently, while two non-resonant objects exchange little energy. That formed a large interest in various sectors of the industry, such as the charging of mobile electric devices. There are many studies on contactless battery charging for mobile phones with a focus on near-field power transmission [4-7]. Additionally, there are approaches by embedding transmitter coils under tables, to hide the system in everyday use [8, 9]. Applications for medical implants, for instance, are also considered to be important due to the difficulties in reaching these implants inside the human body and the associated costs [10-14]. Other applications include mobile laptop charging [15, 16], roadway powered electric vehicles [17, 18], integrated circuit power supplies [19, 20] and even space vehicle operations [21]. Due to that huge amount of applications, industries are establishing and combining wireless power standards, as the Wireless Power Consortium (WPC) with more than 204 members and its Qi standard specification [21-23]. There are also other Associations, like the Power Matters Alliance (PMA) [24, 25] with more than 100 members and the Alliance for Wireless Power (A4WP) [25, 26] with more than 130 members. From the technical point of view, analyzing WPT by using equivalent circuit approaches has become popular [15][27][28-32]. The most recent introduction of WPT technology, is the launch of wireless charging stations at Starbucks and IKEA [33, 34] and also a Qi standard wireless charger introduced by Samsung [35].

There is a big market and a huge interest in finding an easy, cheap and standardized solution for wirelessly charging mobile devices such as mobile phones and electrical vehicle. The challenges, however, lie in the efficiency (and to give the power flow a direction). Previous studies focused on the efficiency of coils when using the resonant technology [36-40]. Meanwhile, majority of the loss happens in the power electronics converter. To enable such resonant-technology based WPT systems, a high-efficiency and high-power-density power electronics system is a must. In cell-phone charging systems, Qi standard requires the switching frequency ~6MHz, exceeding the capability of most Si devices. Wide-bandgap (WBG) devices such as SiC and GaN can increase the resonant frequency to ~MHz level. Such devices are attracting more and more attention due to their high electron mobility, which allows much faster switching transitions thereby reducing switching losses compared to conventional Si devices. This is exemplified by the lowest Figure of merit (R_{DS}(on) x QG) of all power transistor technologies available today as shown in Fig. 1. GaN

Wei Qian is currently a Ph.D. candidate at the School of Mechanical Engineering, Shanghai Jiao Tong University (SJTU), Shanghai, China.

Xi Zhang is currently an associate professor with the Institute of Automotive Engineering and National Engineering Lab for Automotive Electronics and Control Technology, SJTU.

Yongsheng Fu is currently a research assistant in University of Michigan Dearborn.

Juncheng Lu is with GaN Systems Inc, Ottawa, K2K 3G8 Canada (e-mail: llu@gansystems.com).

Hua Bai is with the University of Michigan-Dearborn as associate professor.(e-mai: baihua@umich.edu).

has a high breakdown field [41], approximately ten times higher than that of silicon. For the same breakdown voltage, GaN-based transistors are ~10 times shorter/thinner with respect to the silicon counterpart, and this results in a significant reduction of the on-resistance of the devices. The ultra-fast switching capabilities of GaN, combined with low on-resistance and superior thermal performance, enables higher efficiency and power density in these applications. It has been reported that some applications using GaN HEMTs can push the switching frequency to ~MHz and even hundreds of MHz [42-46], which significantly shrinks passive components, e.g. inductors, capacitors, and potentially resulting in coreless transformers or inductors. This is extremely important especially in when the magnetic core is not preferred due to the weight requirement, e.g., electric scooters. When charging a 48V battery on scooters or a 5V cell-phone battery wirelessly, a heavy receiver equipped with magnetic cores leads to a negative customer experience. Furthermore, faster switching transitions than Si enables a smaller dead time, thus a better PWM resolution and lower harmonic distortion.[41] Most of GaN HEMTs available shown as Table I. Compared to SiC MOSFETs, GaN HEMTs are focused on <650V applications, making it a perfect candidate of low-voltage applications.

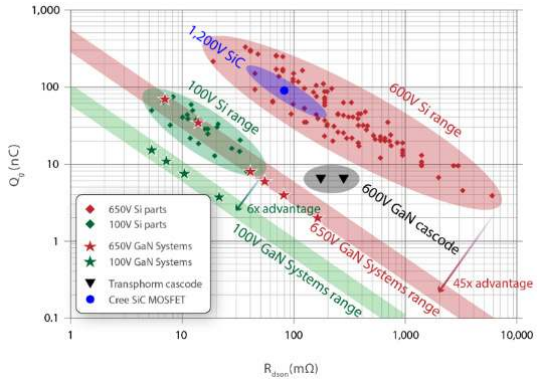

Fig. 1. Merit comparison between different technologies.

TABLE I
POSSIBLE CANDIDATES OF GAN HEMTS

Part Number	Manu-facture	V_{DS} (V)	I_{ds} (A)	R (mΩ)	Gate charge (nC)	Package
GS66516T	GaN Systems	650	60	27	13	GaN Px 9x7.6x0.45
TPH3205WS	Transphorm USA	600	36	52	19	TO247
EPC2034	EPC	200	31	7	8.5	Passivated Die
PGA26E08BA	Panasonic	600	15	56	8.5	DFN 8x8 (BV-Typ)
NTP8G206N	ON Semi-conductor	600	17	150	6.2	TO 220 Style 10
QFN8-HB2-1D	Sanken Electric	600	20	50		QFN 8x8x0.85 (mm)
AVJ199R06060A	Avogy	650		200		TO 220
MGG1T0617D	MicroGaN GmbH	600	30	170	4	Die

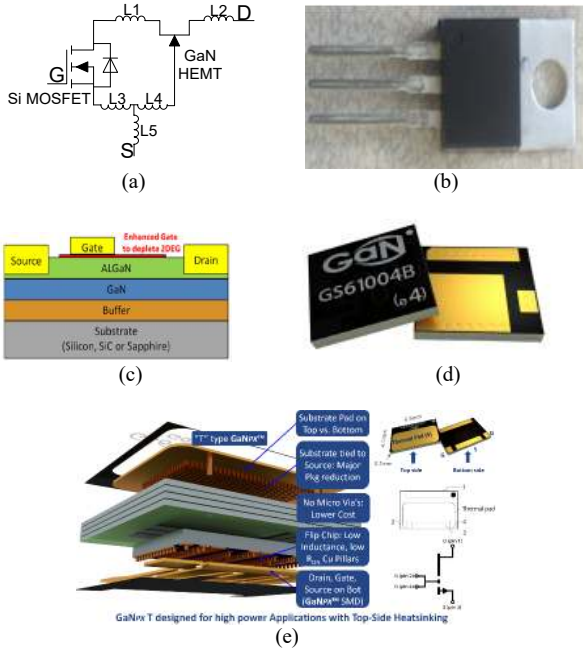

Fig. 2. (a) Cascode GaN HEMT structure (b) TO-220 GaN HEMT provided by Transphorm Inc. (c) enhancement-mode GaN HEMTs (d) package of 100V/30A E-mode GaN HEMTs (e). GaNpxTM packaging.

Both systems adopt Series-Series connection (SSC) resonance topology, shown in Fig. 3(a)~(b). Q1-Q4 are GaN HEMTs. D1~D4 are Schottky diodes. C_p and L_p are the primary-side resonant capacitor and inductor, respectively. C_s and L_s are the secondary-side resonant capacitor and inductor, respectively. L_m is the mutual inductance. R_1 and R_2 are the internal resistance of the primary and secondary coils, respectively. R_L is the equivalent load resistance.

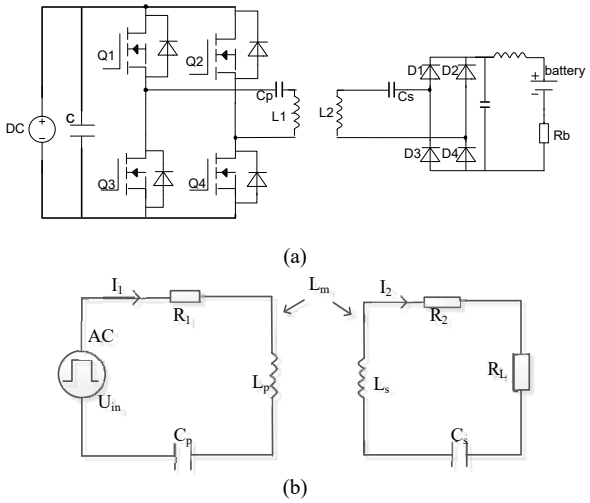

Fig. 3. (a) SSC topology based WPT system (b) Equivalent circuit.

In Section II, a cascode GaN HEMT provided by Transphorm is used to build a 48V/500W wireless charger for the electric scooter. The switching frequency is ~800 kHz. In Section III, an E-mode GaN HEMT provided by GaN Systems Inc. is used to build a 20W multiple-cell-phone wireless charging systems, operated at ~6MHz. Both chargers allow >10cm charging. At the end of each section, the charger

will be compared with Si based version in terms of the efficiency. Section IV is the conclusion. The ultimate goal of this study is not designing the wireless charger, but to 1) demonstrate effectiveness of GaN on eliminating the magnetic core through working at a high switching frequency, 2) increase the efficiency by utilizing the Fig. of merits of GaN HEMTs, and 3) research the challenges and summarize the design rules when using such devices.

II. Case 1: Using Cascode GaN HEMTs In A Single-Receiver System (Electric scooter)

A. Switch Characterization

Before building such WPT on the scooter, it is important to comprehend the switch performance. A double pulse test (DPT) bench, shown as Fig.4 is used. No extra anti-paralleled diode is used, which allows measuring the actual performance of its body diode. Fig. 4(a)~(b) show the DPT test bench. The top signals in Fig.4 (c)~(d) are I_{ds} and V_{ds}, the integral of which represents the turn-on energy (E-on) and turn-off (E-off) energy, measured as 13.8μJ and 6.12 μJ, respectively.

Table II shows the test condition. A brief benchmark indicates that nowadays Si MOSFETs with similar voltage and current ratings have much larger E-on and E-off. Such GaN device provides a much better switching performance, as shown in Table II. Using such device projects a higher efficiency than Si at the same switching frequency.

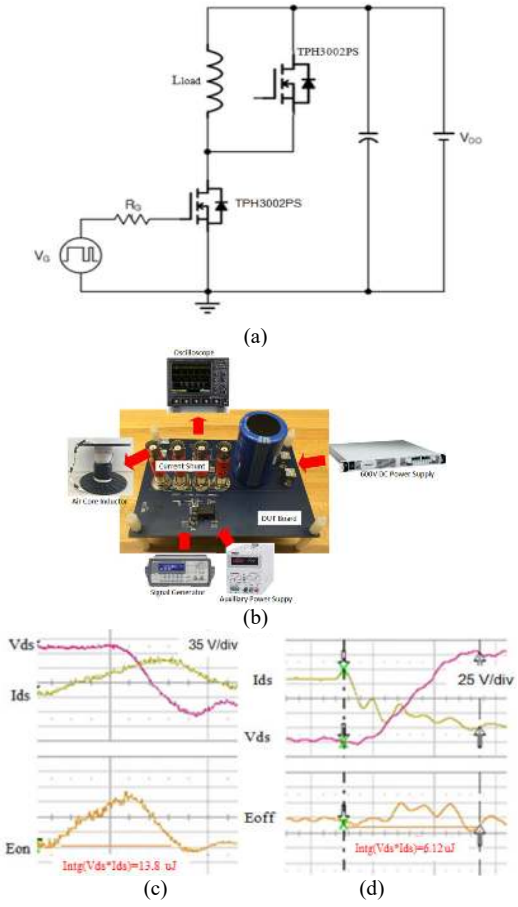

Fig. 4. (a) DPT Circuit (b) DPT Hardware (c) Turn on Waveform (d) Turn off Waveform.

TABLE II
SWITCHING LOSS COMPARISON

Parameter	GaN TPH3002PS	Si MOSFET FQP9N50C
Upper Diode	TPH3002PS	ISL9R1560
Rated Voltage/Current	600 V/ 9 A	500 V/ 9 A
On-Resistance	0.29 Ω	0.8 Ω
Q_g	6.2 nC	28 nC
Test Condition	150V/6A	150V/6A
R_g	8.2 Ω	8.2 Ω
L_{load}	220 uH	220 uH
V_{gs}	+8.1/-3.9V	+12/-5V
E-on/E-off	13.8 uJ/ 6.12 uJ	30 uJ/ 22 uJ
Q_{rr}	29 nC	2.95 μC

B. Coil Design

Furthermore system parameters extracted through ANSYS/Maxwell show the mutual inductance is 5.5156μH and the self-inductances of primary and secondary coils are 30.868μH and 25.619μH, respectively. In addition, the primary coil internal resistance is 210mΩ and the secondary coil internal resistance is 160mΩ. Coil misalignment is also simulated as Fig.5c and d. Since this paper is focused on the effectiveness of GaN HEMTs in WPT systems, optimization of the coils will be not detailed.

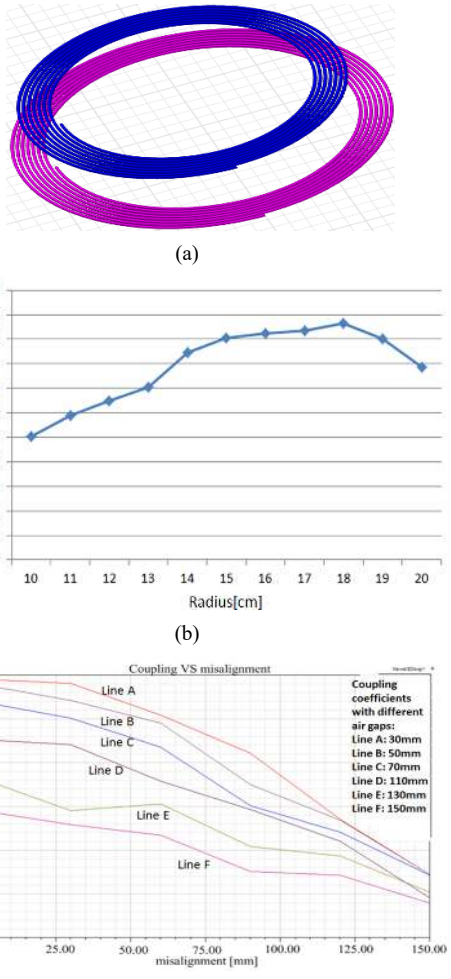

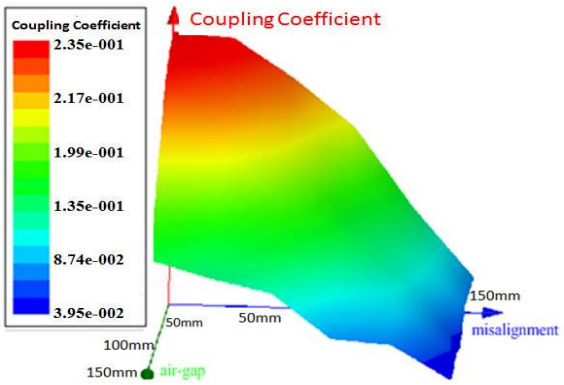

(d)

Fig. 5. (a) Coil Setups in ANSYS (b) Coupling coefficient vs primary coil radius (c) Coupling co-efficient vs misalignment (d) Coupling co-efficient vs misalignment and air-gap.

The resonant capacitances of the primary and secondary side are chosen as 1.77nF and 2nF, respectively using Eqn. (1). It is assumed that the battery is equivalent to a load resistance $R_L=8/(\pi V_o/I_o)$. V_o is the battery terminal voltage, I_o is the battery charging current, $\omega = 2\pi f_s$ and f_s is 800kHz.

$$Z(\omega) = j\omega L_{lp} + \frac{1}{j\omega C_p} + /\left\{ j\omega L_m \,//\, (j\omega L_{ls} + R_L + \frac{1}{j\omega C_s}) \right\} \quad (1)$$

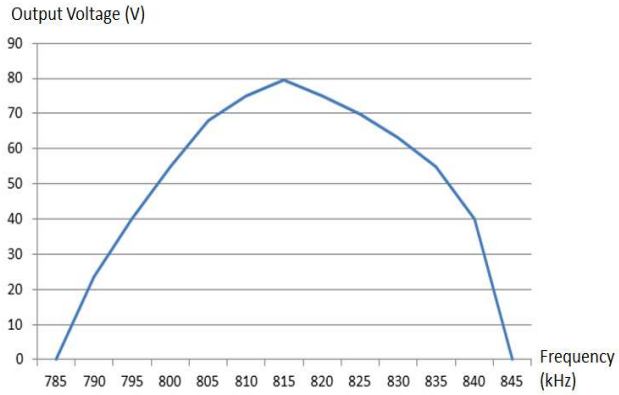

Fig. 6. Voltage gain vs switching frequency.

Fig. 6 shows the relationship between the system output voltage and the switching frequency. The system reaches the peak output voltage when the switching frequency is 813 kHz.

C. Experimental Validation

Fig. 7(a)~(b) show the hardware prototype with detailed parameters shown in Table III. Fig. 7(c) shows the H-bridge output voltage (green) and the primary-coil current waveform (red). Fig. 7(d) shows the V_{gs} (green) and V_{ds} (red) of the GaN device.

(a)

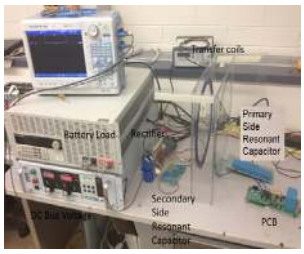

(b)

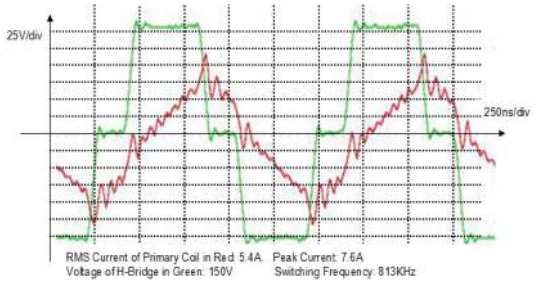

(c)

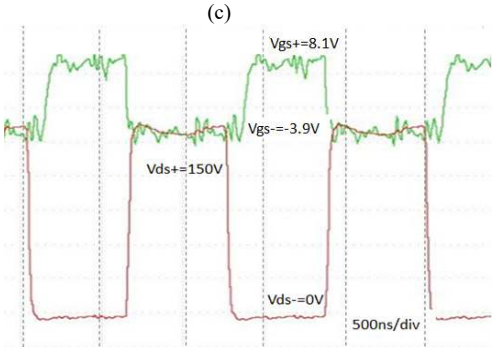

(d)

Fig. 7. (a) Hardware prototype (front side and back side of the PC) (b) Test bench of WPT system (c) Primary H-bridge voltage and current (d) V_{gs} and V_{ds} of one GaN HEMT.

TABLE III
TESTING PARAMETERS OF WPT

Parameter	Value
Switching frequency	813 KHz
Dead time	90 ns
PWM duty cycle	43%
Gate resistance for GaN HEMT	8.2 Ω
Self-inductance of primary side	30.87 uH
Self-inductance of secondary side	25.62 uH
Mutual inductance	5.52 uH
Input DC-bus voltage	150 V
Input average current	1.34 A
Output battery voltage	48 V
Output battery current	3.8 A

The experimental data indicates 90.7% overall system efficiency from the DC input to the battery terminals. The grid-side PFC is not included. As a head-to-head comparison, a CoolMOS with the same voltage and current rating as TPH3002PS was selected to replace GaN HEMTs. Fig. 8 shows the experimental comparison of the total loss under the same output power. The system lost soft switching at 600W. Even so the system loss using GaN is still much lower than CoolMOS. Effectiveness of using GaN HEMTs in this single-Tx-single-Rx wireless charging system is validated.

D. Challenges

Due to the ultra-fast switching speed, the stray inductance in the gate-drive circuit loop needs be extracted and minimized. With the TO-247 package, it is difficult to reduce the gate-drive-loop area and keep all switches having the same-shape gate-drive loop. Shown in Fig. 9(a) and (b) are two different layout for two complementary-switch gate-drive loops, respectively. Modelling in ANSYS/MAXWELL suggests 9.4nH and 25nH loop inductance, respectively. An LTSpice

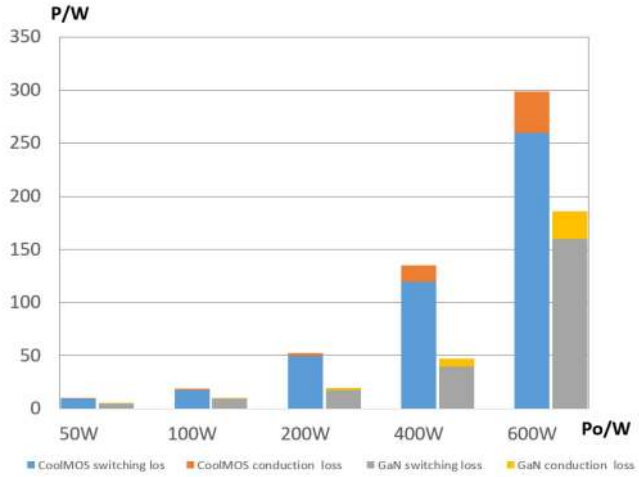

Fig. 8. Experimental loss comparison between CoolMOS and GaN.

model of the GaN HEMT was employed to investigate the impact of gate parameters. Fig 9 (c) show the gate signal V_{gs} with different gate-drive-loop inductance, also it suggest such ringing on the gate will result in the voltage spike across the drain and source. Even though the maximum voltage spike is still far less than 650V, the voltage rating, it is subject to increase the switching-off loss. To further increase the switching frequency and switching speed, a smaller package for reducing the gate-drive-loop area is proposed.

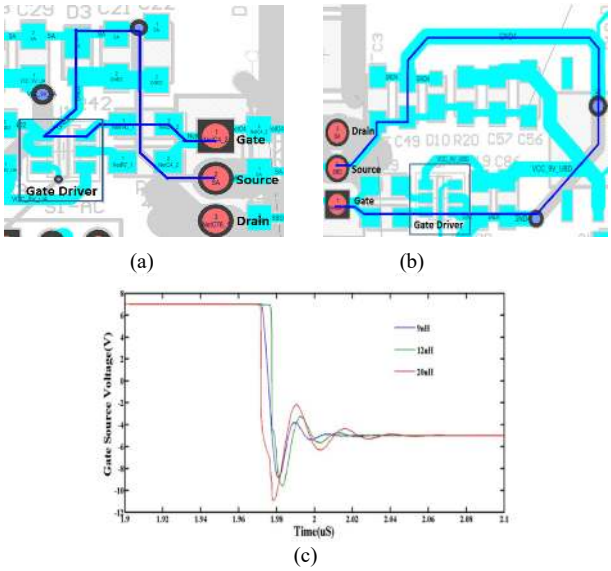

Fig. 9. (a) PCB Gate-drive loop of Q1 (9.45nH) (b) PCB Gate-drive loop of Q2 (25nH) (c) V_{gs} of one GaN HEMT with different loop inductance.

III. Case 2: Using E-Mode GaN HEMTs In A Multiple-Receiver System For Cell-Phone Wireless Charging

The goal of this application is to power multiple cell phones through a wide air gap at 6MHz. Directly using the above TO-247 packaged cascode GaN HEMTs sees the obstacle from the large gate-loop inductance and the reverse recovery loss of the Si-MOSFET body diode. For such application, a 100V enhancement-mode GaN HEMT is a better candidate due to its no-lead package and ultra-small size.

A. Switch characterization

Table.4 shows the parameters of the selected GaN HEMTs. The DPT results for such switch are shown in Fig.10. Given that such switch has no body diodes, no reverse recovery loss is the concern any more. Therefore ZVS is not a must, though still preferred at the high-efficiency application. As shown in Fig.10, such switch does not see the obvious increment of the switching off energy. If possible, employing the ZVS on like Section II will get rid of the switching-on loss thereby reaching high efficiency. Meanwhile the soft switching technology is beneficial to reduce the oscillation on the gate, given that such device gate is fragile. Any V_{GS}>10V tends to break down the switch. The physical package is ¼ of the TO247, which facilitates the system size and parasitic reduction.

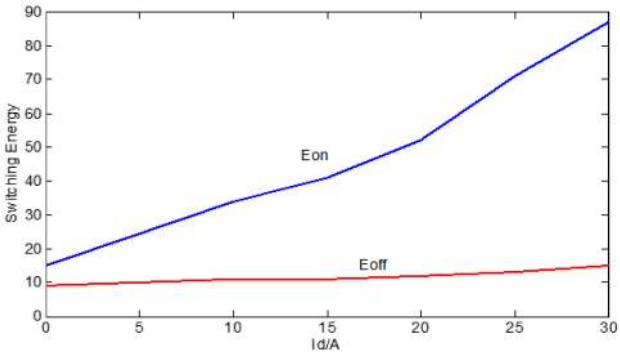

Fig . 10. DPT result of the GS610048.

TABLE IV
PARAMETERS OF GAN HEMTS

PARAMETER	VALUE OR MODEL
GAN HEMT	GS610048
V_{DS} RATING	100 V
I_{DS} RATING	45 A
GATE CHARGE	6.2NC
R_{DSON}	15MΩ
V_{GS}	+7V/-5V

Because of the absence of the body diode, the reverse conduction mode of GaN HEMTs is different from Si MOSFETs, during which the drain and the source will be flipped. When V_{gd} is higher than the reverse threshold voltage V_{th_gd}, the 2-domensional electron gas (2DEG) of GaN HEMTs conducts the current with the voltage drop shown as (2). To minimize the dead-band loss, we used 0V to turn off the switch, i.e., V_{gs_off}=0V. When reverse conducting, it will see ~2V voltage drop.

$$V_{sd} = V_{th\_gd} - V_{gs\_off} + i_d R_{dson} \quad (2)$$

B. Coil Design

To utilize such 100V GaN HEMTs, the grid-side PFC needs step down the grid voltage to some lower voltage, e.g., 50V, then feed such DC voltage to the WPT converter equipped with two resonant coils. From Eqn. (2), due to its larger dead-band voltage drop than cascoded structure, the DC-bus voltage can't be too low, otherwise the dead-band loss will be relatively high.

Fig. 11(a) shows the overall topology of the multi-coil cell-phone charger, where k_{RR} is the coupling coefficient

between the receivers (Rxs) and k_{TR1} and k_{TR2} is the coupling coefficient between the tranceirver (Tx) and two receivers (Rx1 and Rx2), respectively. Another approach is to use two Txs with multiple Rxs, seen in Fig. 11(b). Two Txs are vertical to each other to expand the charging area, shown as Fig.11(c). Assume Rxs1/2 are aligned to Txs1/2, respectively. There are additional coupling coefficients k_{TR12} and k_{TR21} between Tx1 and Rx2 and Tx2 and Rx1, respectively. All the Txs and Rxs are laid out on the PCB to save the cost.

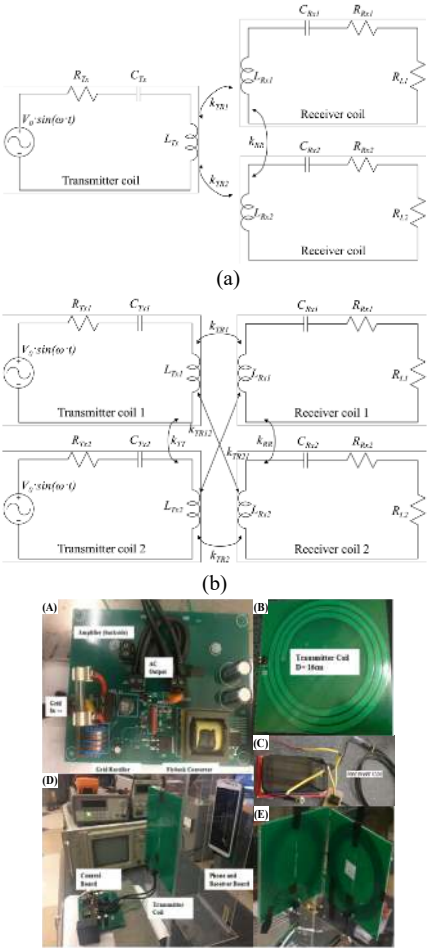

(a) (b) (d)

Fig. 11. (a) multiple Rxs to one Tx. (b) multiple Rxs to multiple Txs. (c) A-Control board, B-Tx coil, C- Rx coil, D-test bench and E-two Tx topology.

TABLE V
MAXWELL SIMULATION RESULTS FOR THE TOPOLOGY IN FIG. 11(D).

MTR1 / μH	MTR2 / μH	MTR12 / μH
0.072622	0.86029	0.012685

MTR21 / μH	MTT / μH	MRR / μH
0.010911	0.290073	0.001483

Assume the phones are perfected aligned with their own coils. In this test, phone 2 is fixed at *d2* = 10 cm and the distance *d1* of phone 1 is varied between 5 and 18 cm. The system is always operated at the resonant frequency. An overview and the results are shown in Fig. 12(a). As seen in the two-Tx-two-Rx system, there is a fight between the Rxs for the charging power. The phone 1 receives the most of the power when it is close to the Tx and then gradually loses the power to phone 2.

To investigate such behavior, self inductance and mutual inductance are obtained from Ansys/Maxwell, as seen in Fig. 12(b). To make the analysis more general, we randomly placed the Rxs at different locations and angles. Introduction of the second Rx will slightly alter the mutual inductance between Txs and Rxs. However since the system is very frequency selective, even such a tiny variation could result in the power change. By applying the inductance variation in LTSpice, powers are simulated to prove the power performance in the tests is in the right way, seen in Table VI.

Such power fighting among receivers is difficult to solve, given the fact that the mutual inductance will be changed when the second or even more receivers are introduced. One effective method is to increase the input DC-bus voltage, which will increase the charging power for all receivers simultaneously. When one cell phone is fully charged, the battery inside the phone will be disconnected from the charging system, which allows other phones to keep getting charged.

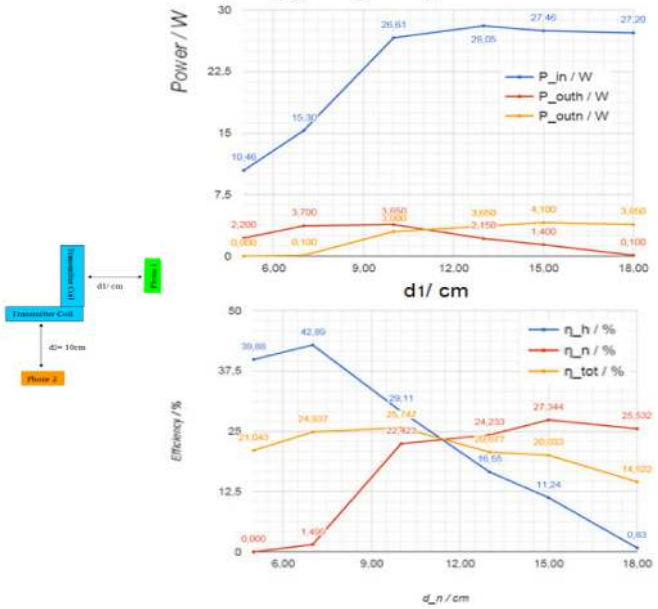

(a)

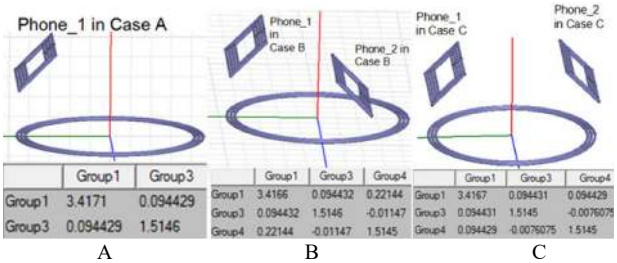

(b)

Fig. 12. (a) Two Txs to two Rxs. (b) Simulations results for self and mutual inductance.

TABLE VI
LTSPICE SIMULATION RESULTS FOR THE POWER IN THE MENTIONED CASES A-C.

Param.	P1_A	P1_B	P2_B	Ptot_B	P1_C	P2_C	Ptot_C
Sim. Value	3.4 W	0.9 W	3.1 W	4.0 W	1.6 W	2.2 W	3.8 W
Test Value	3.1 W	0.75 W	3.0 W	3.75 W	1.5 W	2.0 W	3.5 W

C. Experimental Validation

As the head-to-head comparison with silicon devices, an AC-DC converter supplied by the grid is designed to provide a constant voltage (V_{CC}) to the DC-AC amplifier IXRFD630, shown as Fig. 11(a) using silicon technology. C_{rx1v} is another capacitor to tune the resonant frequency. The system is designed to charge mobile phones with a large freedom of movement to realize an easy and user-friendly wireless charging when users are interacting with a phone or leave the phone on a specific surface. The amplifier is able to generate a signal with a frequency of around 6.78 MHz to provide the resonator, which is made up by a Tx coil and an impedance matching network. A secondary impedance matching network, a rectifier and a DC-DC converter are connected to Rx coil to charge a phone with a constant 5 V power supply. We define this design as Alpha version. Such a 5V power supply (DC-DC Converter in Fig.13) also applies to the GaN version. As the comparison, 100V GaN HEMTs are used with the topology shown in Fig.2a, which is defined as Beta version.

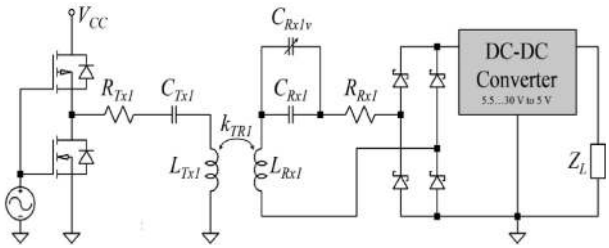

Fig. 13. Alpha version using Amplifier IXRFD630.

When testing both versions, the DC-bus voltage is varied thereby changing the charging power. Such solution won't solve the power fighting, however will increase all charging power together. An experimental comparison is shown as below, which indicated that using GaN solutions has a much higher efficiency and power than the conventional Si solution. Fig.14 shows gate signals of the complementary switches on the same leg. Even though slightly distorted, the switch duty cycle is still maintained ~50%@~6MHz. Table.VII shows the GaN-version WPT has much higher efficiency than Si version. Note such efficiency is measured from the V_{CC} shown as Fig.13 to the phone battery.

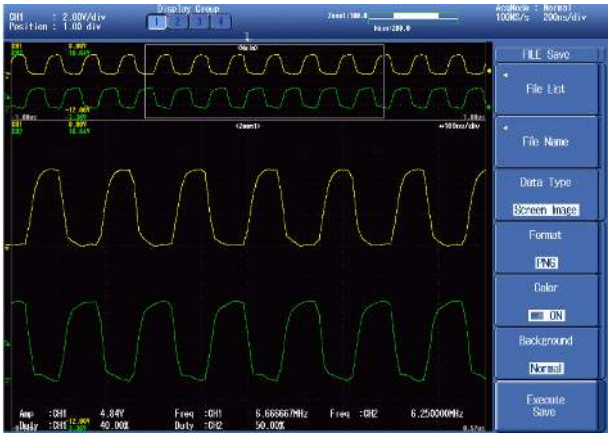

Fig. 14. The gate signals of two complimentary GaN HEMTs in the same leg.

TABLE VII
COMPARISON OF SI VERSION AND GAN VERSION WPT

Parameters	Alpha Version	Beta Version
Topology	Push-pull	GaN H-Bridge
Phone 1 Distance	5 cm	5 cm
Phone 2 Distance	10 cm	10 cm
Phone 1 Charging V/I/P	5V/0.44A/2.2W	5V/0.88A/4.4W
Phone 2 Charging V/I/P	5V/0.1A/0.5W	5V/0.6A/3W
Efficiency	21%	36.7%

D. Challenges

To minimize the gate-drive loop inductance and the cross talking between the gate-drive loop and power loop, the Kelvin terminal is usually employed especially in the bottom-cooled GaN HEMTs. Once the higher current is needed, paralleling switches is required, which encounters the problem brought by the common-source inductance. As shown in Fig.15, the loop current could be described as Eqn. (3). The induced ringing on the gate voltage of HEMT 1 and HEMT 2 is shown as Eqns. (4) and (5), respectively. Here i_{loop} means the current circulating among paralleled switches.

$$Ls1\frac{di_1}{dt} - Ls2\frac{di_2}{dt} = i_{loop} * (Zss1 + Zss2) \tag{3}$$

$$V_{feedback\_1} = Zss1\frac{Ls1\frac{di_1}{dt} - Ls2\frac{di_2}{dt}}{Zss1 + Zss2} \tag{4}$$

$$V_{feedback\_2} = Zss2\frac{Ls1\frac{di_1}{dt} - Ls2\frac{di_2}{dt}}{Zss1 + Zss2} \tag{5}$$

Shown in Fig.15b, a 1nH difference between the common-source inductance (Ls1 and Ls2) of two paralleled GaN HEMTs will result in the huge ringing on the gate, which will mis-trigger switches or damage the gate. One possible solution is a diverse-parameter based gate-drive circuit shown in Fig.15c. Instead of using the same gate-drive resistance, we purposely placed a bigger gate-resistance for one switch, e.g., HEMT 2. When turned on, since they are all ZVS turned on, the different turn-on speed will not affect the switching-on behaviors. When turned off, HEMT1 will first turn off at ZVS condition since HEMT2 is still on. The gate ringing will be fully eliminated.

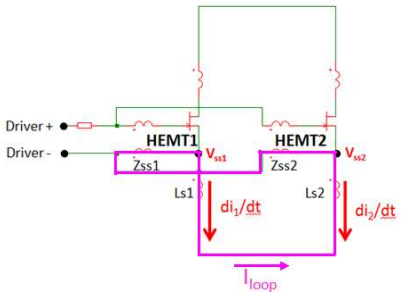

(a)

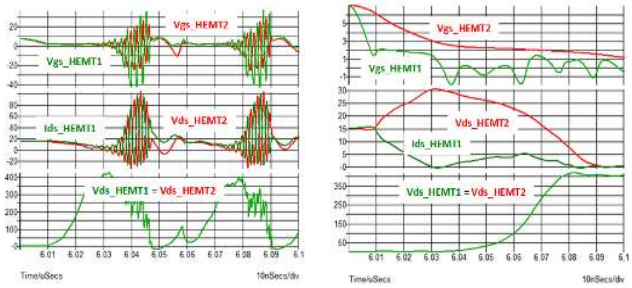

(b) (c)

Fig. 15. (a) Equivalent Circuit of Paralleled GaN HEMTs. (b) Gate-drive Signals Based on the Conventional Gate-Drive Method. (c) Gate-Drive Signals Based on the Proposed Gate-Drive Method.

A multi-layer PCB could significantly reduce parasitic of both the gate-drive loop and power loop by the magnetic-flux-canceling technique, i.e., the direction of the commutation current on two adjacent layers are opposite so that the generated flux outside the loop gets cancelled. Compared to the direct-bonded-copper (DBC) substrate, the PCB design could easily adopt the multi-layer structure with smaller loop area to achieve an excellent magnetic flux canceling effect. As shown in Fig.16, The decoupling cap in located under the top and bottom switches to minimize the loop area, which in return reduces the loop inductance. Such a half bridge with four GaN HEMTs in parallel is modeled in ANSYS Q3D, and the power-loop and gate-drive-loop inductance are evaluated by Finite Element Analysis (FEA). The power-loop inductance of the proposed design is only 0.7 nH. For each paralleled GaN HEMT, its quasi-common source inductance is <0.2 nH.

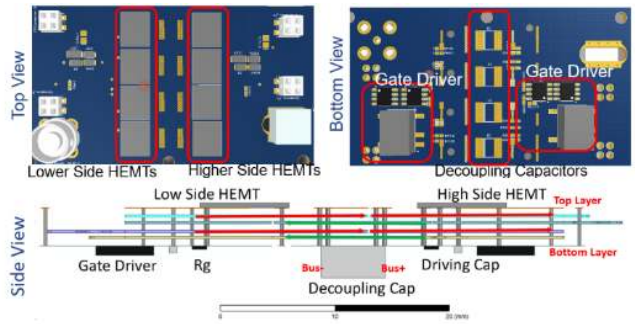

Fig. 16. Layout of GaN HEMTs Using Flux Cancelling.

IV. Conclusions

In this paper, a high-frequency wireless charging system for the electric scooter application using normally-off GaN HEMTs is designed. > 90% system efficiency was achieved with ~800 kHz switching frequency. Power up to 600 W was realized. The switching performance of cascode GaN HEMT has been evaluated by both the simulation and experiments with power loss analysis given as well.

Effectiveness of GaN Systems' E-mode devices is also validated by a cell-phone wireless charging case, where two cell phones could be charged together. Efficiency of using GaN is nearly double of that Si version. 6.6MHz switching is realized.

Overall, experimental results indicated that the performance of GaN HEMTs is superior to the conventional Si devices. For both applications, we increase the switching frequency so as to save the space of the coils, reduce the resonant capacitor to nF level and eliminate the ferrite cores. Such devices also have their own challenges, e.g., gate-drive-loop and quasi-common-mode inductance might affect its reliability and parallel. Flux cancelling technique is briefly discussed, which is critical when paralleling switches.

The GaN devices provided by Transphorm has conventional TO-247 packages. The long leads and large dies introduces higher parasitics, which limit its switching frequency to <1MHz. However, the large die area enhances the thermal capability, which makes it well positioned in the high-power applications. For GaN Systems' 100V GaN devices, the compact design reduces the parastics significantly, which explains why the charger can go beyond 6MHz. The small thermal area needs be paid attention. In the real practice, we usually use multiple in parallel to enlarge the sufficient heatsink area.

References

[1] Nikola Tesla; U.S. Patent 0,645,576; March 20, 1900; https://www.google.de/patents/US649621

[2] Nikola Tesla; U.S. Patent 0,645,576; December 1, 1914; https://www.google.com/patents/US1119732

[3] A. Kurs, A. Karalis, R. Moffatt, J. D. Joannopoulos, P. Fisher, and M. Soljacic, "Wireless power transfer via strongly coupled magnetic resonances," *Science*, vol. 317, no. 5834, pp. 83–86, Jul. 2007.

[4] Y. Jang and M. M. Jovanovic, "A contactless electrical energy transmission system for portable-telephone battery chargers," *IEEE Trans. Ind. Electron.*, vol. 50, no. 3, pp. 520–527, Jun. 2003.

[5] B. Choi, J. Nho, H. Cha, T. Ahn, and S. Choi, "Design and implementation of low-profile contactless battery charger using planar printed circuit board windings as energy transfer device," *IEEE Trans. Ind. Electron.*, vol. 51, no. 1, pp. 140–147, Feb. 2004.

[6] C.-G. Kim, D.-H. Seo, J.-S. You, J.-H. Park, and B. H. Cho, "Design of a contactless battery charger for cellular phone," *IEEE Trans. Ind. Electron.*, vol. 48, no. 6, pp. 1238–1247, Dec. 2001.

[7] J. Hirai, T.-W. Kim, and A. Kawamura, "Study on intelligent battery charging using inductive transmission of power and information," *IEEE Trans. Power. Electron.*, vol. 15, no. 2, pp. 335–345, Mar. 2000.

[8] K. Hatanaka, F. Sato, H. Matsuki, S. Kikuchi, J. Murakami, M. Kawase, and T. Satoh, "Power transmission of a desk with a cord-free power supply," *IEEE Trans. Magn.*, vol. 38, no. 5, pp. 3329–3331, Sep. 2002.

[9] J. Murakami, F. Sato, T. Watanabe, H. Matsuki, S. Kikuchi, K. Harakawa, and T. Satoh, "Consideration on cordless power station—Contactless power transmission system," *IEEE Trans. Magn.*, vol. 32, no. 5, pp. 5037–5039, Sep. 1996.

[10] G. A. Kender, W. Liu, G. Wang, M. Sivaprakasam, R. Bashirullah, M. S. Humayun, and J. D. Weiland, "An optimal design methodology for inductive power link with class-E amplifier," *IEEE Trans. Circuits Syst. I, Reg. Papers,* vol. 52, no. 5, pp. 857–865, May 2005.

[11] A. K. RamRakhyani, S. Mirabbasi, and M. Chiao, "Design and optimization of resonance-based efficient wireless power delivery systems for biomedical implants," *IEEE Trans. Biomed. Circuits Syst.*, vol. 5, no. 1, pp. 48–63, Feb. 2011.

[12] M. P. Theodoridis and S. V. Mollov, "Distant energy transfer for artificial human implants," *IEEE Trans. Biomed. Eng.*, vol. 52, no. 11, pp. 1931–1938, Nov. 2005.

[13] M. Kiani and M. Ghovanloo, "An RFID-based closed-loop wireless power transmission system for biomedical applications," *IEEE Trans. Circuits Syst. II, Exp. Briefs*, vol. 57, no. 4, pp. 260–264, Apr. 2010.

[14] M. Sawan, S. Hashemi, M. Sehil, F. Awwad, M. Hajj-Hassan, and A. Khouas, "Multicoils-based inductive links dedicated to power up

implantable medical devices: Modeling, design and experimental results," *Biomed. Microdevices*, vol. 11, no. 5, pp. 1059–1070, Jun. 2009.

[15] A. P. Sample, D. T. Meyer, and J. R. Smith, "Analysis, experimental results, and range adaptation of magnetically coupled resonators for wire- less power transfer," *IEEE Trans. Ind. Electron.*, vol. 58, no. 2, pp. 544–554, Feb. 2011.

[16] J. A. Taylor, Z. N. Low, J. Casanova, and J. Lin, "A wireless power station for laptop computers," in *Proc. IEEE Radio Wireless Symp.*, 2010, pp. 625–628.

[17] C. S. Wang, O. H. Stielau, and G. A. Covic, "Design considerations for a contactless electric vehicle battery charger," *IEEE Trans. Ind. Electron.*, vol. 52, no. 10, pp. 1308–1314, Oct. 2005.

[18] S. Lee, J. Huh, C. Park, N.-S. Choi, G.-H. Cho, and C.-T. Rim, "On-line electric vehicle using inductive power transfer system," in *Proc. IEEE Energy Convers. Congr. Expo.*, 2010, pp. 1598–1601.

[19] F. Segura-Quijano, J. Garcia-Canton, J. Sacristan, T. Oses, and A. Baldi, "Wireless powering of single-chip systems with integrated coil and external wire-loop resonator," *Appl. Phys. Lett.*, vol. 92, no. 7, pp. 074102-1074102-3, Feb. 2008.

[20] K. Onizuka, H. Kawaguchi, M. Takamiya, T. Kuroda, and T. Sakurai, "Chip-to-chip inductive wireless power transmission system for SiP applications," *in Proc. IEEE Custom Integr. Circuits Conf.*, 2006, pp. 575–578.

[21] R. J. Sedwick, "Long range inductive power transfer with superconducting oscillators," *Ann. Phys.*, vol. 325, no. 2, pp. 287–299, Feb. 2010.

[22] "System description wireless power transfer,"*Wireless* Power Consortium Standards, Apr. 2011.

[23] S. Y. Hui, "Planar Wireless Charging Technology for Portable Electronic Products and Qi," *Proceedings of the IEEE*, Vol. 101, no. 6, pp. 1290-1301, June 2013.

[24] http://www.powermatters.org/

[25] Minseok Han; Ji-Min Kim; Hoon Sohn, "Dual-mode wireless power transfer module for smartphone application," in *Antennas and Propagation & USNC/URSI National Radio Science Meeting*, 2015 IEEE International Symposium on , vol., no., pp.111-112, 19-24 July 2015

[26] R. Tseng, B. V. Novak, S. Shevde and K. A. Grajski, "Introduction to the Alliance for Wireless Power Loosely-Coupled Wireless Power Transfer System Specification Version 1.0," *IEEE Wireless Power Transfer Conference 2013, Technologies, Systems and Applications*, Perugia, Italy, May 2013.

[27] Z. N. Low, R. A. Chinga, R. Tseng, and J. Lin, "Design and test of a high-power high-efficiency loosely coupled planar wireless power transfer system," *IEEE Trans. Ind. Electron.*, vol. 56, no. 5, pp. 1801–1812, May 2009.

[28] T. Imura and Y. Hori, "Maximizing air gap and efficiency of magnetic resonant coupling for wireless power transfer using equivalent circuit and Neumann formula," *IEEE Trans. Ind. Electron.*, vol. 58, no. 10, pp. 4746–4752, Oct. 2011.

[29] S. Cheon, Y.-H. Kim, S.-Y. Kang, M. L. Lee, J.-M. Lee, and T. Zyung, "Circuit model based analysis of a wireless energy transfer system via coupled magnetic resonances," *IEEE Trans. Ind. Electron.*, vol. 58, no. 7, pp. 2906–2914, Jul. 2011.

[30] M. W. Baker and R. Sarpeshkar, "Feedback analysis and design of RF power links for low-power bionic systems," *IEEE Trans. Biomed. Circuits Systs.*, vol. 1, no. 1, pp. 28–38, Mar. 2007.

[31] M. Kiani, U.-M. Jow, and M. Ghovanloo, "Design and optimization of a 3-coil inductive link for efficient wireless power transmission," *IEEE Trans. Biomed. Circuits Syst.*, vol. 5, no. 6, pp. 579–591, Dec. 2011.

[32] M. Kiani and M. Ghovanloo, "The circuit theory behind coupled-mode magnetic resonance-based wireless power transmission," *IEEE Trans. Circuits Syst.* I, Reg. Papers, to be published.

[33] Tekla Perry, "Starbucks, Ikea Enter the Wireless Charging Fray," *IEEE SPECTRUM*, http://spectrum.ieee.org/view-from-the-valley/consumer-electronics/standards/starbucks-ikea-enter-the-wireless-charging-fray, 25 March 2015, 14:00 GMT.

[34] IKEA, http://www.ikea.com/us/en/catalog/categories/departments/wireless_charging/, 2015.

[35] SAMSUNG, http://www.samsung.com/za/consumer/mobile-devices/accessories/power/EP-PG920IBEGWW, 2015.

[36] Wenxian Chen; Qianhong Chen; Juntao Huang; Huijuan Zhang, "Analysis and Research of Distance Transmission Characteristics of Magnetic Resonance WPT System," i*n Vehicular Technology Conference (VTC Spring)*, 2014 IEEE 79th , vol., no., pp.1-5, 18-21 May 2014.

[37] FU Wen-zhen, ZHANG Bo, QIU Dong-yuan, WANG Wei. "Maximum Efficiency Analysis and Design of Self-resonance Coupling Coils for WPT System" .*Proceedings of the CSEE*.2009, 29(18):21-26.

[38] Ning Yin; Guizhi Xu; Qingxin Yang; Jun Zhao; Xuewen Yang; Jianqiang Jin; Weinong Fu; Mingui Sun, "Analysis of Wireless Energy Transmission for Implantable Device Based on Coupled Magnetic Resonance," in *Magnetics, IEEE Transactions* on , vol.48, no.2, pp.723-726, Feb. 2012.

[39] LI Feng-e. "Circuit Parameter Analysis of Maximum Transfer Distance of Magnetic Resonance WPT Systems". *Journal of nanchang hangkong university (natural sciences)*,2012,26(3):48-62.

[40] Dukju Ahn; Songcheol Hong, "Effect of Coupling Between Multiple Transmitters or Multiple Receivers on Wireless Power Transfer," in I*ndustrial Electronics, IEEE Transactions* on, vol.60, no.7, pp.2602-2613, July 2013.

[41] Chongwen Zhao, Daniel Costinett, "GaN-Based, Dual-Mode Wireless Power Transfer Using Multi-Frequency Programmed Pulse Width Modulation", *IEEE Trans. Ind. Electron.*, Volume: PP, Issue: 99, pp. 1 - 1, March 2017.

[42] Z.Y. Liu, X.C. Huang, Fred C. Lee, Q. Li, "Simulation Model Development and Verification for High Voltage GaN HEMT in Cascode Structure", *IEEE Energy Conversion Conference and Expo*, 2013, pp. 1-4.

[43] X.C. Huang, Q. Li, Z.Y. Liu, Fred C. Lee, "Analytical Loss Model of High Voltage GaN HEMT in Cascode Configuration", *IEEE Energy Conversion Conference and Expo*, 2013, pp.3587-3594.

[44] W.M. Zhang, Z.X. Xu, Z.Y. Zhang, Fred Wang,. Leon M. Tolbert, "Evaluation of 600V Cascode GaN FEMT in Device Characterization and All-GaN-Based LLC Resonant Converter", *IEEE Energy Conversion Conference and Expo*, 2013, pp. 3571-3578.

[45] Yuanzhe Zhang, Miguel Rodr´ıguez and Dragan Maksimovi´c, "100 MHz, 20 V, 90% Efficient Synchronous Buck Converter with Integrated Gate Driver", *IEEE Energy Conversion Conference and Expo*, 2014, pp.3664-3671.

[46] Matteo Meneghini, Isabella Rossetto, Carlo De Santi, "Reliability and failure analysis in power GaN-HEMTs: An overview," in *IEEE International Reliability Physics Symposium (IRPS)*, 2017.

Wei Qian received the B.S. degree in Mechanical Engineering and Automation from Nanjing University of Aeronautics & Astronautics (NUAA), Nanjing, China, in 2005 and the M.S. degree in Aircraft Design from Nanjing University of Aeronautics & Astronautics (NUAA), Nanjing, China, in 2013. He is currently a Ph.D. candidate at the School of Mechanical Engineering, Shanghai Jiao Tong University (SJTU), Shanghai, China.

His research interests include soft switching power converters, power electronics devices and electric motor control systems.

Xi Zhang received the B.Sc. degree in Applied Mathematics and the B.E. degree in Information and Control Engineering from Shanghai Jiao Tong University (SJTU), Shanghai, China in 2002. He received the M.E. and Ph.D. degrees in Power Electronics and Electric Power Drive from SJTU, in 2004 and 2007, respectively. From September 2007 to July 2009, he held a postdoctoral position with the Department of Electrical and Computer Engineering, the University of Michigan-Dearborn, Dearborn, MI, USA. He is currently an associate professor with the Institute of Automotive Engineering and National Engineering Lab for Automotive Electronics and Control Technology, SJTU. His research interests include power management strategies, power electronics devices and electric motor control systems for alternative-fuel vehicles.

Yongsheng Fu Received the B.S. and M.S. Degrees from Xi'an Technological University ShannXi, 2010 and 2013, respectively. Research Scholar in Kettering University from 2013 to 2014. He is currently a research assistant in University of Michigan Dearborn. His research interests include power electronics, detection and auto control.

Juncheng Lu received B S degree from Zhejiang University., Hangzhou, China in 2011 , and M.S. degree from Kettering University, Michigan, USA. in 2016. From 2011~2014, he was a Research Engineer at Delta Power Electronics Center, Shanghai, China. Since 2016, he has been an Applications Engineer at GaN Systems, Inc., Ottawa, Canada. He holds 7.U.S. Patents(or Pending). His research interest is high power density power supply integration, wide band gap devices application, power module, and electrical vehicle battery charger.

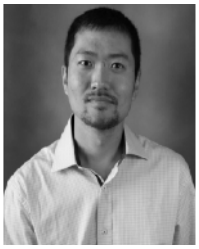

Hua BAI received B S and PHD degree in Department of Electrical Engineering of Tsinghua University., Beijing, China in 2002 and 2007, respectively. He was a post-doc fellow and research scientist in Univ of Michigan-Dearborn, USA, in 2007 and 2009, respectively. He was an assistant professor in Department of Electrical and Compurter Engineering, Kettering University, MI, USA in 2010~2016. From 2017 he joined University of Michigan-Dearborn as associate professor. His research interest is the power electronic modelling, control and integration including variable frequency motor drive system, high voltage and high power DC/DC converter, wide-bandgap devices and hybrid electric vehicles.